RESEARCH PAPER



Layout optimization of multi-type dampers in structures under seismic excitation

Zhihao Ou¹ · Baisheng Wu¹ · Siu-Kai Lai² · Zeyao Chen¹

Received: 28 January 2025 / Revised: 3 September 2025 / Accepted: 6 September 2025 / Published online: 29 September 2025 © The Author(s) 2025

Abstract

Seismic performance is a critical consideration in the design of building structures to maintain its stability and strength. One effective approach to enhance this performance is the installation of dampers. However, traditional design methods often fail to achieve the optimal arrangement of dampers for improving seismic resilience. This paper presents an optimization method for determining the most effective layout of multi-type dampers based on bidirectional evolutionary structural optimization (BESO). The optimization objective is to minimize the maximum variance of inter-story drift across all floors, given a specified maximum number of each type of damper. To approximate the non-smooth objective function, the Kreisselmeier—Steinhauser (KS) function is incorporated. In addition, an efficient algorithm based on the pseudo excitation method (PEM) is introduced to calculate the frequency-domain stochastic seismic response of non-proportionally damped structures throughout the layout optimization process. Two frame structure examples are presented to illustrate the application and effectiveness of the proposed method.

Keywords Layout optimization · Non-proportional damping · Stochastic seismic excitation · Pseudo excitation method · Iteration method

1 Introduction

In civil engineering, it is important to ensure the seismic performance of structures. One effective approach to enhance earthquake resistance is by installing damper devices in structures (Housner et al. 1997; Soong and Spencer 2002; Symans et al. 2008). Using a sufficient number of various damper types can reliably meet performance requirements, but this solution is not cost-effective. Therefore, when the maximum number of each damper type is given, determining the optimal layout arrangement of multiple damper types is the focus of seismic design research. However, traditional

Responsible Editor: Qing Quan Liang.

- Siu-Kai Lai sk.lai@polyu.edu.hk
- School of Electro-Mechanical Engineering, Guangdong University of Technology, Guangzhou 510006, People's Republic of China
- Department of Civil and Environmental Engineering, The Hong Kong Polytechnic University, Kowloon, Hong Kong, People's Republic of China

design methods often struggle to effectively identify the most effective layout of dampers, making it challenging to achieve optimal seismic performance.

Topology optimization is an effective method to achieve the optimal layout of materials in a specified design domain according to certain constraints and objective functions (Bendsøe and Kikuchi 1998). In recent years, the topology optimization of damper layouts for structures under seismic excitation has emerged as a prominent area of research. Lavan and Amir (2014) took the damping coefficient of each potential viscous damper as a continuous variable and determined it through a topology optimization algorithm. Subsequently, Pollini et al. (2017) further extended this study to the case of nonlinear viscous dampers. Gomez et al. (2021) simultaneously optimized the structure layout and damping coefficient by solving a Lyapunov equation. However, incorporating dampers with different damping coefficients within the same structure remains a technical issue for engineering applications. Based on the equivalent linearization method and the time-domain explicit approach, Su et al. (2016) developed an effective time-domain random vibration analysis method for nonlinear structures subjected to non-stationary random excitation, which was subsequently

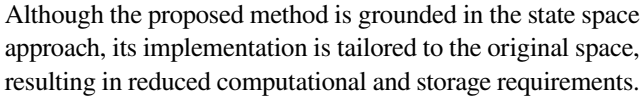


206 Page 2 of 19 Z. Ou et al.

applied to the layout optimization of nonlinear viscous dampers in building structures under non-stationary random seismic excitation (Su and Xian 2022). It is important to note that varying initial layouts can result in substantial differences in the final outcomes, making it challenging to attain a genuinely optimal damper arrangement.

Although nonlinear considerations are often taken into account when designing structures under seismic excitation, in most cases standard design practice assumes that the behavior of the structure is linear (Gomez et al. 2021). Therefore, in this study, we assume that the structural model is linear. In calculating the stationary seismic response of a structure, the pseudo excitation method (PEM) is a typical frequency-domain analysis method that converts a stationary seismic process into a simple harmonic process (Lin et al. 2001; Li et al. 2023). However, the addition of dampers yields a non-proportionally damped system. For non-proportionally damped system, the damping matrix no longer satisfies the modal orthogonal condition. At the same time, attention should be directed toward structural responses across the entire seismic frequency range, rather than concentrating on just a particular frequency. The complex mode superposition method (CMSM) (Traill-Nash 1981) is the most widely used technique for analyzing the structural dynamic behavior of non-proportionally damped systems. Indeed, CMSM necessitates the availability of all complex modes. Obtaining these complex modes is nearly impossible, particularly for large-scale problems. As a result, modal truncation must be implemented, which can significantly impact the accuracy of the results. To overcome the shortcomings of CMSM, a hybrid expansion method (HEM) (Liu et al. 1996; Huang et al. 1997; Qu 2000; Qu and Selvam 2000; Li et al. 2014, 2016) based on modal superposition and power series expansion of the dynamic flexible matrix has been proposed. However, a key question is how many terms of the power series expansion need to be retained to achieve the desired level of accuracy. In addition, using HEM requires calculations at each frequency of interest within the specified frequency range.

To efficiently analyze the dynamic behavior of non-proportionally damped systems within a frequency range, Wu et al. (2022) proposed a non-proportionally damped frequency response method (NPDFRM). The method can adaptively determine which lower-order mode to calculate, while the influence of the unknown higher-order modes on the frequency response is estimated using the partial sum of a convergent power series. The iterative algorithm is executed only at the right end of the excitation frequency interval, and the number of terms in the partial sum can be determined adaptively. The derived frequency response expression is valid across the entire range of excitation frequencies. Consequently, by varying the excitation frequency in the analytical expression, the response for the entire frequency range can be readily obtained.



Controlling lateral drift in structures is a crucial regulatory aspect of seismic design (International Conference of Building Officials 1997; European Committee for Standardization 2004; National Standard of the People's Republic of China 2010). Minimizing the maximum variance of interstory drift across all floors leads to a more uniform distribution of inter-story drift ratios along the building height (Alavi and Krawinkler 2004). A structure with uniformly distributed inter-story drift ratios is generally more resilient to seismic events compared to traditional structures, as it can reduce localized damage and distribute seismic forces more evenly (Moghaddam et al. 2005). In this work, an optimization method based on BESO is proposed to determine the layout of multi-type dampers in structures under stationary seismic excitation. The goal is to minimize the maximum inter-story drift variance among all floors, given a specified maximum number of each type of damper. This method starts with the full layout of dampers as the initial design, thereby avoiding the issue of different final results caused by variations in the initial damper layout configuration. This method combines PEM with NPDFRM to calculate the interstory drift variance of a non-proportionally damped structure, which makes stochastic seismic response more accurate and the calculation process simpler and more economical. At the same time, the Kreisselmeier-Steinhauser (KS) function (Kreisselmeier and Steinhauser 1979) is then employed to minimize the maximum inter-story drift variance among all floors to achieve the optimal layout of multi-type dampers.

In what follows, Sect. 2 presents the preparatory work, which includes PEM and NPDFRM. Section 3 offers comprehensive explanation to the layout optimization framework based on the BESO method. Section 4 provides two examples of frame structures to demonstrate the effectiveness of the proposed algorithm, and Sect. 5 concludes with final remarks.

2 Preparatory work

The dynamic equation of a structure system with N_{DOF} degrees of freedom under seismic excitation can be expressed as:

$$\mathbf{M}\ddot{\mathbf{x}}(t) + \mathbf{C}\dot{\mathbf{x}}(t) + \mathbf{K}\mathbf{x}(t) = -\mathbf{M}\mathbf{I}a_g(t)$$
(1)

where $\mathbf{M} \in \mathbb{R}^{N_{DOF} \times N_{DOF}}$ is the global mass matrix; $\mathbf{C} \in \mathbb{R}^{N_{DOF} \times N_{DOF}}$ is the global damping matrix; $\mathbf{K} \in \mathbb{R}^{N_{DOF} \times N_{DOF}}$ is the global stiffness matrix; $\mathbf{x}(t)$ denotes an N_{DOF} -dimensional displacement vector and a dot represents the differentiation with respect to time t; \mathbf{I} is an N_{DOF} -dimensional vector whose components are equal to 1 for the



DOFs corresponding to the main horizontal direction of the earthquake effect and 0 for all others; and $a_g(t)$ is the ground acceleration generated by seismic excitation. In this work, the floor mass is modeled as a lumped mass and distributed across all beam-column nodes of the structure (Gao et al. 2022). The mass value of each node is set as m_n .

In Eq. (1), the damping matrix cannot be diagonalized. To solve this equation, the auxiliary equation $\mathbf{M}\dot{\mathbf{x}} - \mathbf{M}\dot{\mathbf{x}} = 0$ is introduced to obtain

$$\mathbf{A}\mathbf{y} + \mathbf{B}\dot{\mathbf{y}} = \mathbf{r}a_g(t) \tag{2a}$$

where

$$\mathbf{A} = \begin{bmatrix} \mathbf{K} & \mathbf{0} \\ \mathbf{0} & -\mathbf{M} \end{bmatrix}, \ \mathbf{B} = \begin{bmatrix} \mathbf{C} & \mathbf{M} \\ \mathbf{M} & \mathbf{0} \end{bmatrix}, \ \mathbf{y} = \begin{bmatrix} \mathbf{x} \\ \dot{\mathbf{x}} \end{bmatrix}, \ \mathbf{r} = \begin{bmatrix} -\mathbf{M}\mathbf{I} \\ \mathbf{0} \end{bmatrix}$$
 (2b)

Based on PEM (Lin et al. 2001), the ground acceleration can be expressed as

$$a_g(t) = \sqrt{S_g(\omega)}e^{i\omega t}, \omega \in [0, \omega_{\text{max}}]$$
 (3)

where $S_g(\omega)$ represents the power spectral density (PSD) function of the seismic excitation. In this paper, the structure is subjected to a ground motion described by the Clough–Penzien (C–P) mode (Clough and Penzien 1975) where $S_g(\omega)$ is given by

$$S_{g}(\omega) = S_{0} \frac{1 + 4\xi_{g}^{2} \left(\frac{\omega}{\omega_{g}}\right)^{2}}{\left[1 - \left(\frac{\omega}{\omega_{g}}\right)^{2}\right]^{2} + 4\xi_{g}^{2} \left(\frac{\omega}{\omega_{g}}\right)^{2}} \times H_{f}(\omega), \omega \in \left[0, \omega_{\text{max}}\right]$$

$$(4a)$$

where

$$H_f(\omega) = \frac{\left(\frac{\omega}{\omega_f}\right)^4}{\left[1 - \left(\frac{\omega}{\omega_f}\right)^2\right]^2 + 4\xi_f^2 \left(\frac{\omega}{\omega_f}\right)^2} \tag{4b}$$

and S_0 is the spectral intensity coefficients of seismic excitation; ξ_g and ω_g are the damping ratio and frequency of the site soil, respectively; and $H_f(\omega)$ is a low frequency filter in which ξ_f and ω_f are the damping ratio and frequency of the filter, respectively.

Setting $\mathbf{y}(t) = \mathbf{Y}e^{i\omega t}$ in Eqs. (2a), (2b) and (3) yields

$$(\mathbf{A} + i\omega \mathbf{B})\mathbf{Y} = \mathbf{R}, \omega \in [0, \omega_{\text{max}}], \quad \mathbf{R} = \begin{bmatrix} -\mathbf{M}\mathbf{I}\sqrt{S_g(\omega)} \\ \mathbf{0} \end{bmatrix}$$
(5)

The process of NPDFRM for solving Eq. (5) is briefly reviewed herein, we refer readers to (Wu et al. 2022) for details. According to NPDFRM (Wu et al. 2022), we define the following interval

$$\left[0, \lambda_r\right] = \left[0, \omega_{\text{max}}/\theta\right] \tag{6}$$

where θ is an optional positive parameter (<1). Using NPD-FRM (Wu et al. 2022) can compute the required the low-order modes $\Psi_L = \left[\psi_1, \psi_2, \dots, \psi_l \right]$ where the corresponding frequencies fall within the interval specified in Eq. (6).

According to CMSM, the solution $\mathbf{Y}(\omega)$ in Eq. (5) can be written as

$$\mathbf{Y}(\omega) = \mathbf{\Psi}_L \mathbf{e}_L(\omega) + \mathbf{U}(\omega) \tag{7}$$

where $\mathbf{e}_L(\omega) = \left(e_1(\omega), e_2(\omega), \cdots, e_l(\omega)\right), \quad e_s(\omega) = \frac{\mathbf{\psi}_s^T \mathbf{R}}{i\omega - \lambda_s}$ ($s = 1, 2, \dots, l$) and $\mathbf{U}(\omega)$ is the contribution from the uncalculated high-order modes. The unknown part $\mathbf{U}(\omega)$ can be solved by using the following iterative formula

$$\mathbf{U}_{k+1} = \mathbf{G}(\omega)\mathbf{U}_k + \mathbf{b}, \ \mathbf{U}_0 = 0, \ k = 0, 1, 2, ..., \ \omega \in [0, \omega_{\text{max}}]$$
(8)

where

$$\mathbf{G}(\omega) = -i\omega \mathbf{A}^{-1} \Big[\mathbf{B} - \mathbf{B} \mathbf{\Psi}_L \big(\mathbf{B} \mathbf{\Psi}_L \big)^{\mathrm{T}} \Big], \ \mathbf{b} = \mathbf{A}^{-1} \big(\mathbf{R} - \mathbf{B} \mathbf{\Psi}_L \mathbf{\Psi}_L^{\mathrm{T}} \mathbf{R} \big)$$
(9)

It should be emphasized that the spectral radius $\mathbf{r}(\omega)$ of matrix $\mathbf{G}(\omega)$ is smaller than θ , so the iteration in Eq. (8) converges.

Equation (8) can be rewritten as

$$\mathbf{U}_{k+1}(\omega) = \sum_{j=0}^{k} a^{j} \mathbf{p}_{j}, \ a = \omega / \omega_{\text{max}}, \ \omega \in \left[0, \omega_{\text{max}}\right]$$
 (10)

and the vectors $\mathbf{p}_0, \mathbf{p}_1, \dots, \mathbf{p}_k$ are determined by using the following recurrence relation

$$\mathbf{A}\mathbf{p}_{0} = \mathbf{R} - \mathbf{B}\mathbf{\Psi}_{L}\mathbf{\Psi}_{L}^{\mathrm{T}}\mathbf{R}$$

$$\mathbf{A}\mathbf{p}_{j} = -i\omega_{\max}[\mathbf{B} - \mathbf{B}\mathbf{\Psi}_{L}(\mathbf{B}\mathbf{\Psi}_{L})^{\mathrm{T}}]\mathbf{p}_{j-1}, \ j = 1, 2, \dots$$
(11a)

The stopping criterion of the algorithm is

$$\frac{\left\|\mathbf{p}_{j}\right\|_{2}}{\left\|\sum_{q=0}^{j}\mathbf{p}_{q}\right\|_{2}} < \delta_{m} \tag{11b}$$

where δ_m is the preset tolerance. For details, please refer to Wu et al. (2022).

To enhance the efficiency of solving Eq. (11a), NPDFRM

converts the solution from state space to primal space as fol- $\begin{bmatrix} x_1 \end{bmatrix}$

lows with
$$\mathbf{p}_j = \begin{bmatrix} \mathbf{p}_j^1 \\ \mathbf{p}_j^2 \end{bmatrix}$$

$$\begin{bmatrix} \mathbf{K}\mathbf{p}_{j}^{1} \\ -\mathbf{M}\mathbf{p}_{j}^{2} \end{bmatrix} = -i\omega_{\max} \left[\mathbf{B} - \mathbf{B}\mathbf{\Psi}_{L} (\mathbf{B}\mathbf{\Psi}_{L})^{T} \right] \begin{bmatrix} \mathbf{p}_{j-1}^{1} \\ \mathbf{p}_{j-1}^{2} \end{bmatrix}, \ j = 1, 2, \dots$$
(12)



206 Page 4 of 19 Z. Ou et al.

Equation (12) can be further partitioned into the following two uncoupled systems

$$\begin{cases} \mathbf{K}\mathbf{p}_{j}^{1} = -i\omega_{\max}(\mathbf{C}\mathbf{g}_{1} + \mathbf{M}\mathbf{g}_{2}) \\ \mathbf{p}_{i}^{2} = i\omega_{\max}\mathbf{g}_{1} \end{cases}, \ j = 1, 2, \dots$$
 (13)

where

$$\begin{split} \boldsymbol{\Psi}_{L} &= \begin{bmatrix} \boldsymbol{\Psi}_{L}^{1} \\ \boldsymbol{\Psi}_{L}^{1} \boldsymbol{\Lambda}_{L} \end{bmatrix}, \; \boldsymbol{\Psi}_{L}^{\mathrm{T}} = \begin{bmatrix} \boldsymbol{\Psi}_{L}^{1\,\mathrm{T}} \; \boldsymbol{\Lambda}_{L} \; \boldsymbol{\Psi}_{L}^{1\,\mathrm{T}} \end{bmatrix}, \\ \begin{bmatrix} \boldsymbol{h}_{1} \\ \boldsymbol{h}_{2} \end{bmatrix} &= \boldsymbol{B} \boldsymbol{p}_{j-1} = \begin{bmatrix} \boldsymbol{C} \boldsymbol{p}_{j-1}^{1} + \boldsymbol{M} \boldsymbol{p}_{j-1}^{2} \\ \boldsymbol{M} \boldsymbol{p}_{j-1}^{1} \end{bmatrix}, \end{split}$$

$$\begin{bmatrix} \mathbf{f}_1 \\ \mathbf{f}_2 \end{bmatrix} = \mathbf{\Psi}_L \mathbf{\Psi}_L^T \mathbf{B} \mathbf{p}_{j-1} = \begin{bmatrix} \mathbf{\Psi}_L^1 \big(\mathbf{\Psi}_L^{1T} \mathbf{h}_1 \big) + \mathbf{\Psi}_L^1 \boldsymbol{\Lambda}_L \big(\mathbf{\Psi}_L^{1T} \mathbf{h}_2 \big) \\ \mathbf{\Psi}_L^1 \boldsymbol{\Lambda}_L \big(\mathbf{\Psi}_L^{1T} \mathbf{h}_1 \big) + \mathbf{\Psi}_L^1 \boldsymbol{\Lambda}_L^2 \big(\mathbf{\Psi}_L^{1T} \mathbf{h}_2 \big) \end{bmatrix},$$

$$\begin{bmatrix} \mathbf{g}_1 \\ \mathbf{g}_2 \end{bmatrix} = \begin{bmatrix} \mathbf{p}_{j-1}^1 - \mathbf{f}_1 \\ \mathbf{p}_{j-1}^2 - \mathbf{f}_2 \end{bmatrix}.$$

Solving the systems above separately yields the solution to Eq. (12).

The approximation to Eq. (7) can be written as

$$\mathbf{Y}^{a}(\omega) \approx \mathbf{\Psi}_{L} \mathbf{e}_{L}(\omega) + \mathbf{Pz}(\omega), \ \omega \in [0, \omega_{\text{max}}]$$
 (14)

where

$$\mathbf{P} = \left[\mathbf{p}_0, \mathbf{p}_1, \cdots, \mathbf{p}_k \right], \ \mathbf{z}(\omega) = \left(1, a, a^2, \cdots, a^k \right)^{\mathrm{T}}$$
 (15)

The relative error (RE)

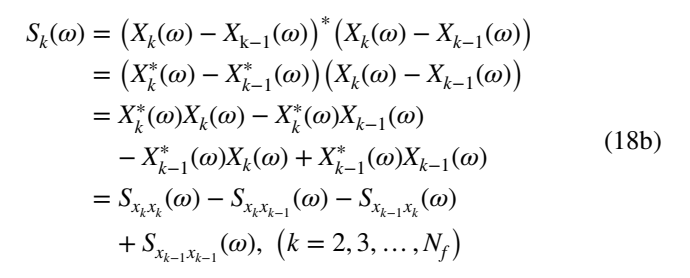
$$RE(\omega) = \frac{\|\mathbf{X}^{a}(\omega) - \mathbf{X}^{f}(\omega)\|_{2}}{\|\mathbf{X}^{f}(\omega)\|_{2}}$$
(16)

is employed to evaluate the accuracy of the approximated seismic response \mathbf{X}^a (the top half of \mathbf{Y}^a), where \mathbf{X}^f is the seismic response calculated by using the direct method (DM) to solve the following system

$$\left(\mathbf{K} + i\omega\mathbf{C} - \omega^2\mathbf{M}\right)\mathbf{X}^f = -\mathbf{M}\mathbf{I}\sqrt{S_g(\omega)}, \omega \in \left[0, \omega_{\text{max}}\right] \quad (17)$$

Using the solution to Eq. (5), we get the PSD function of the k-th story drift (Lin et al. 2001; Liu and Paavola 2015)

$$S_1(\omega) = X_1(\omega)^* X_1(\omega) (k = 1)$$
 (18a)



where $X_k(\omega)$ is the lateral displacement of the structure boundary columns relative to the ground at the k-th floor, $X_k^*(\omega)$ is the complex conjugate of $X_k(\omega)$, and N_f is the total number of floors in the structure.

3 Layout optimization process

The multi-material BESO approach is a topology optimization method that iteratively removes and adds elements to achieve an optimal structural design. Compared with other methods, the BESO approach starts with a complete layout of dampers as the initial design, avoiding the problem of different final results due to the change of the initial damper layout configuration. This characteristic makes it particularly suitable for optimizing the layout of dampers in building structures, as explored in this paper. In combination with the random response algorithm of non-proportionally damped structures under seismic excitation discussed in the previous section, we use the multi-material optimization method based on BESO (Huang and Xie 2009) to determine the layout of multi-type dampers in structures subjected to a specified maximum number of each type of damper. In this paper, the KS function (Kreisselmeier and Steinhauser 1979) is utilized to minimize the maximum inter-story drift variance among all floors:

$$Min \quad J = J_0 \left(1 + \frac{1}{\gamma} \ln \left(\sum_{k=1}^{N_f} e^{\gamma \left(\frac{J_k}{J_0} - 1 \right)} \right) \right),$$

$$J_k = 2 \int_0^{\omega_{\text{max}}} S_k(\omega) d\omega, \ (k = 1, 2, \dots, N_f)$$

$$s.t. \quad g_j(\rho_{ej}) = \sum_{e=1}^{n_e} \rho_{ej} \le M_j, \ (j = 1, 2, \dots, N_t - 1)$$

$$\rho_{ej} \in \{ \rho_{\text{min}}, 1 \}$$

$$(19)$$

where ρ_{ej} represents the density of damper e with the j-th damping parameter; $\rho_{\min} = 0.001$ is the lower boundary of ρ_{ej} ; J_0 is an arbitrary scalar that satisfies $J_0 \ge \max \left(J_k\right)$; γ is a positive weight factor; N_f represents the total number of floors; J_k and $S_k(\omega)$ are the variance (Wirsching et al. 2006) and PSD function of the k-th story drift, respectively; n_e is



the total number of dampers; $g_i(\rho_{ei})$ is the total number of the j-th type of dampers installed; M_i represents the maximum number of the j-th type of dampers; and N_t denotes the number of types of dampers.

The subinterval subdivision technique (Liu et al. 2015), along with the Gauss-Legendre integration method with 8 Gaussian points, is used to calculate the integral in Eq. (19). In the N, types of dampers case and the corresponding damping coefficients are $c_1 > c_2 > \cdots > c_N$. The damping interpolation functions between two adjacent damper types are as follows (Huang and Xie 2009)

$$c(\rho_{ej}) = \rho_{ej}^p c_j + (1 - \rho_{ej}^p) c_{j+1}, (j = 1, 2, \dots, N_t - 1)$$
 (20)

where p is the penalty factor.

We assume that the design variable ρ_{ei} changes from 1 to ρ_{\min} continuously. The derivative of the objective function in Eq. (19) is calculate by using the adjoint variable method (Haftka and Gürdal 1992; Yan and Cheng 2018; Zhao et al. 2021, 2022; Pozo et al. 2023; Ou et al. 2025):

$$\frac{\partial J}{\partial \rho_{ej}} = \sum_{k=1}^{N_f} \frac{\partial J}{\partial J_k} \frac{\partial J_k}{\partial \rho_{ej}}, \quad (j = 1, 2 \dots N_t - 1)$$
 (21)

where

$$\frac{\partial J}{\partial J_k} = \frac{e^{\gamma \left(\frac{J_k}{J_0} - 1\right)}}{\sum_{k=1}^{N_f} e^{\gamma \left(\frac{J_k}{J_0} - 1\right)}}$$
(22a)

$$\begin{split} \frac{\partial J_{k}}{\partial \rho_{ej}} &= 2 \int_{0}^{\omega_{\text{max}}} \frac{\partial S_{k}(\omega)}{\partial \rho_{ej}} d\omega = 2 \int_{0}^{\omega_{\text{max}}} \left[\frac{\partial S_{x_{k}x_{k}}(\omega)}{\partial \rho_{ej}} - \frac{\partial S_{x_{k}x_{k-1}}(\omega)}{\partial \rho_{ej}} - \frac{\partial S_{x_{k-1}x_{k}}(\omega)}{\partial \rho_{ej}} + \frac{\partial S_{x_{k-1}x_{k-1}}(\omega)}{\partial \rho_{ej}} \right] d\omega \end{split}$$

$$(22b)$$

$$\frac{\partial S_{x_k x_{k-1}}(\omega)}{\partial \rho_{ej}} = \int_0^{\omega_{\text{max}}} \left[X_k^*(\omega) \frac{\partial X_{k-1}(\omega)}{\partial \rho_{ej}} + X_{k-1}^*(\omega) \frac{\partial X_k(\omega)}{\partial \rho_{ej}} \right] d\omega$$
(22c)

$$\frac{\partial X_k(\omega)}{\partial \rho_{ej}} = \mathbf{L}_k^{\mathrm{T}} \frac{\partial \mathbf{X}(\omega)}{\partial \rho_{ej}} = -\mathbf{L}_k^{\mathrm{T}} \mathbf{S}^{-1} \frac{\partial \mathbf{S}}{\partial \rho_{ej}} \mathbf{X}(\omega) = -\lambda_k^{\mathrm{T}} \frac{\partial \mathbf{S}}{\partial \rho_{ej}} \mathbf{X}(\omega)$$
(22d)

$$\frac{\partial \mathbf{S}}{\partial \rho_{ej}} = i\omega \cdot p \rho_{ej}^{p-1} (\mathbf{c}_j - \mathbf{c}_{j+1}); \tag{22e}$$

in which \mathbf{L}_k is a column vector of 1 at the term s and 0 elsewhere, where s represents the lateral displacement freedom of the boundary column at the k – th floor of the structure: $\mathbf{S} = \mathbf{K} + i\omega \mathbf{C} - \omega^2 \mathbf{M}$ denotes the dynamic stiffness matrix; λ satisfies $S\lambda_k = L_k$ and can be calculated by using NPDFRM introduced in Sect. 2; and \mathbf{c}_i and \mathbf{c}_{i+1} denote the elemental damping matrices calculated using the damping coefficients

 c_i and c_{i+1} , respectively. Other derivatives in Eq. (22b) can be obtained in a similar way to Eqs. (22c), (22d) and (22e).

The sensitivity number used in the BESO method can be defined by the relative ranking of the sensitivity of an individual element as (Huang and Xie 2009)

$$\frac{\partial \overline{J}}{\partial \rho_{ei}} = -\frac{1}{p} \frac{\partial J}{\partial \rho_{ei}} \tag{23}$$

To ensure the stability of the iterative process, the sensitivity information from the previous two iterations is added to the sensitivity of the current q-th iteration (Huang and Xie 2009), denoted as:

$$\frac{\partial \overline{J}}{\partial \rho_{ej}}^{(q)} = \frac{1}{3} \left(\frac{\partial \overline{J}}{\partial \rho_{ej}}^{(q)} + \frac{\partial \overline{J}}{\partial \rho_{ej}}^{(q-1)} + \frac{\partial \overline{J}}{\partial \rho_{ej}}^{(q-2)} \right)$$
(24)

The evolution of the number of dampers at each iteration is defined as (Chen et al. 2023)

$$N_{a}^{(q+1)} = N_{a}^{(q)}(1 - ER) \tag{25}$$

where $N_e^{(q)}$ represents the total number of dampers at the q-th iteration, and ER is the evolutionary ratio.

The optimization process terminates when the constraint function and the convergence criteria are satisfied. The convergence criterion is (Huang and Xie 2009)

$$\frac{\sum_{i=1}^{M} \overline{J}^{(q-i+1)} - \sum_{i=1}^{M} \overline{J}^{(q-M-i+1)}}{\sum_{i=1}^{M} \overline{J}^{(q-i+1)}} \le \eta$$
 (26)

where q represents the current number of iterations, and Mis an integer. Normally, M is set to 5, which means that the change in average objective function over the last 10 iterations is small enough; η is the default tolerance. For more information on the BESO approach, readers may refer to Huang and Xie (2009). The flowchart of the optimization process is presented in Fig. 1.

When the initial design incorporates all dampers, the nonconvexity of the optimization problem enables BESO to converge to a local optimum solution. Therefore, we introduce a diversified design technique based on the random coefficient penalty method of element sensitivity (Xie 2025) to make the optimization result closer to the global optimum solution. The diversified design technique can be expressed as follows

$$\frac{\partial \tilde{J}}{\partial \rho_{ej}} = \delta_e \frac{\partial \tilde{J}}{\partial \rho_{ej}}, \delta_e \in [1 - \varepsilon, 1 + \varepsilon],
(e = 1, 2, \dots, n_e; j = 1, 2, \dots, N_t - 1)$$
(27)



206 Page 6 of 19 Z. Ou et al.

where $\frac{\partial \bar{J}}{\partial \rho_{ej}}$ is the penalized sensitivity; $\frac{\partial \bar{J}}{\partial \rho_{ej}}$ is the original sensitivity and is calculated using Eq. (23); δ_e is the penalty coefficient of damper e, randomly selected from the range $[1 - \varepsilon, 1 + \varepsilon]$ and ε is set to 0.15 (Xie 2025).

Note that the penalization of element sensitivities is conducted at each iteration. As a result, the ranking of elements based on their sensitivities is altered, influencing the removal or addition of 'marginal' elements with initially low sensitivities, while elements with higher sensitivities are more likely to be retained in the final design (Xie 2025). Due to the random nature of the penalization, this increases the likelihood that the final result will get closer to the global optimum solution.

4 Numerical examples

In this section, two examples are utilized to illustrate the effectiveness of the proposed approach. A workstation equipped with an Intel CPU i9-12900K and 64 GB of RAM performs calculations, and the code is written using MATLAB version: 9.7.0 (R2019b). Both the mass and stiffness matrices are represented in sparse matrix format. In the following examples, we define the random response tolerance of the non-proportionally damped structure as $\delta_m = 10^{-6}$, and set the optional parameter $\theta = 0.5$. For C-P model, we set $\omega_{\rm max} = 20$ Hz, $S_0 = 0.0068 \, m^2 / s^3$, $\xi_g = 0.6$, $\omega_g = 8\pi \, rad/s$, $\xi_f = 0.6$ and $\omega_f = 1.5 \, rad/s$. For the steel frame structure, we set the material parameters of Poisson's ratio v = 0.3, mass density $\rho = 7800 \,\mathrm{kg}/m^3$, Young's modulus $E = 210 \times 10^9$ Pa. The mass value m_n of each node is considered in three cases: 600 kg, 2200 kg and 3000 kg, corresponding to real-world timber floors, steel sheeting and concrete floors, and reinforced concrete floors, respectively (D'Amico and Pomponi 2020). The Rayleigh damping model of the frame structure is adopted with a damping ratio $\xi_c = 0.02$ (Chopra 1995). For layout optimization, the parameter J_0 is set as the maximum value of J_k in each step, and the parameter γ starts with a value of one and it is updated one unit each 25 iterations (Pozo et al. 2023). The convergence criterion tolerance is set as $\eta = 10^{-5}$, the penalty factor is set as p = 3, and the evolutionary ratios is set as ER = 2% (Chen et al. 2023).

4.1 Example 1: 2D frame structure

In this example, we consider a 2D 10-bay, 30-story steel frame structure, as shown in Fig. 2. In Fig. 2a, the frame structure is depicted without dampers, while Fig. 2b shows the structure equipped with full dampers. Each horizontal and vertical black line shown in Fig. 2 represents a beam with a length of 3 m. The cross-section of the beam is

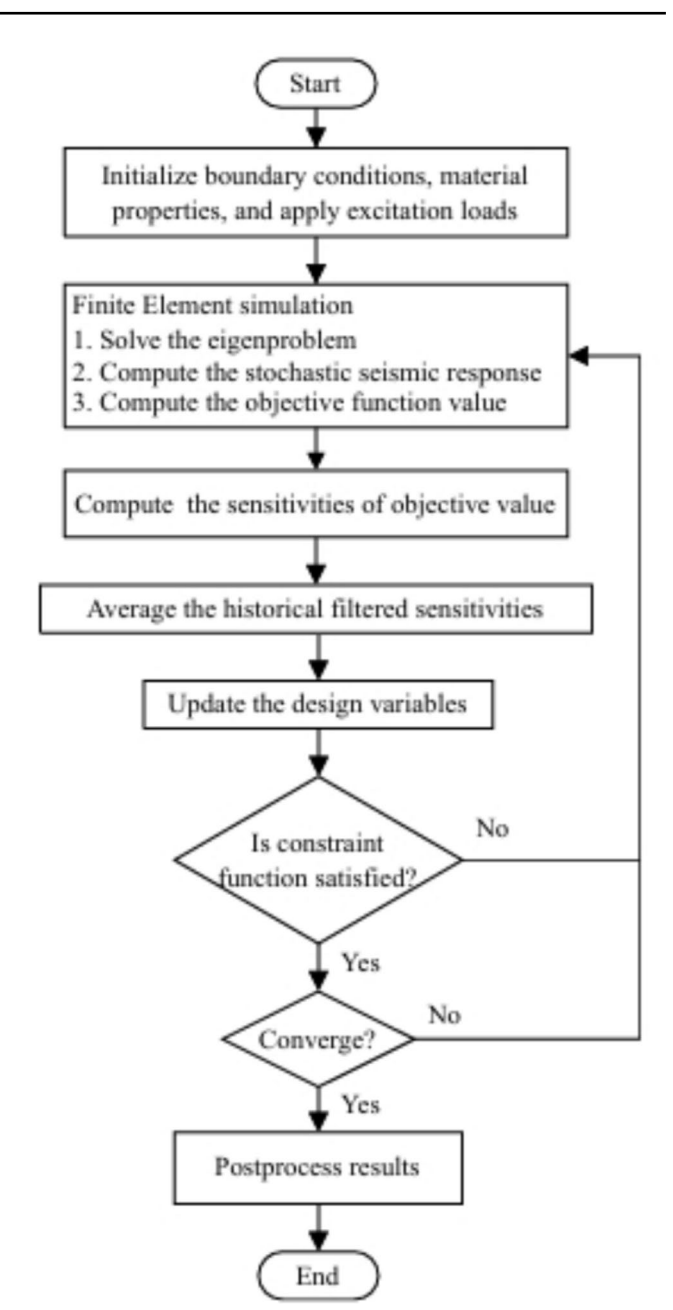
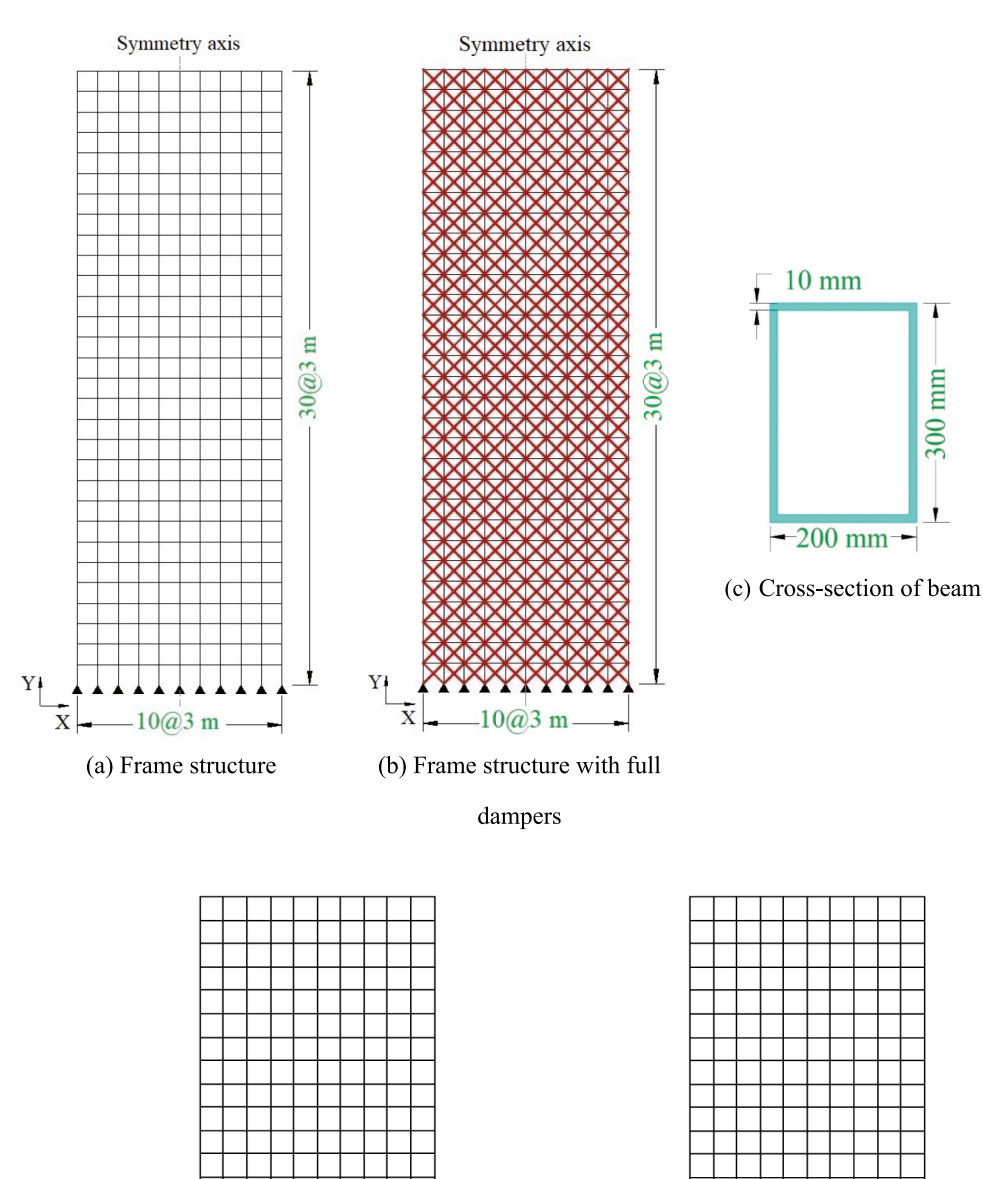


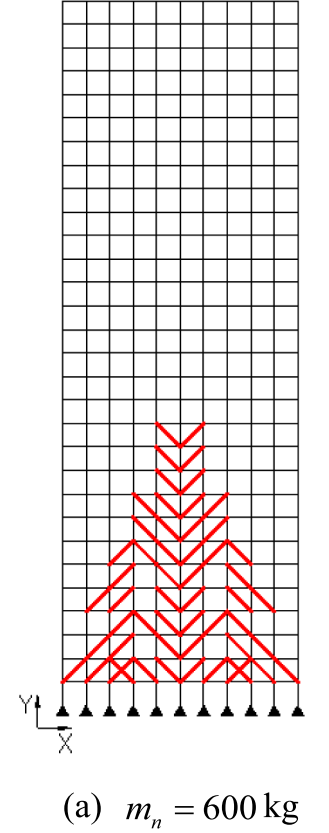
Fig. 1 Flowchart of the optimization process

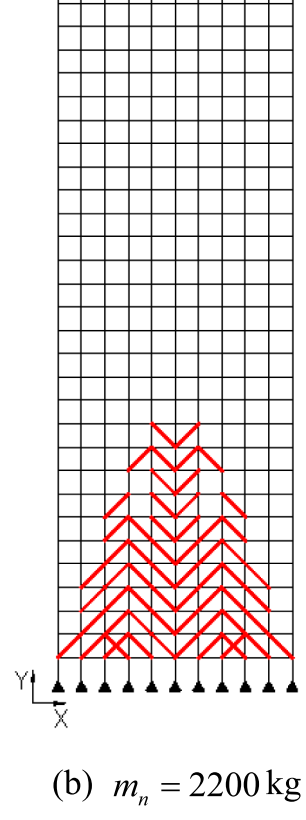
shown in Fig. 2c. Each red line in Fig. 2b represents a viscous damper with damping parameter $c_1 = 1 \times 10^6 \, \mathrm{N} \cdot s/m$. In this structure, the dampers with a vertical span of one floor and a horizontal span of one bay are installed. The number of full dampers in the structure is 600. The finite element model based on Timoshenko beam elements of the structure has 1023 DOFs. In this example, we consider the layout optimization of the structure containing a single type of damper. The number of dampers used is constrained to less than 10% of the number of full dampers, and the seismic excitation is along the X-axis. The proposed method

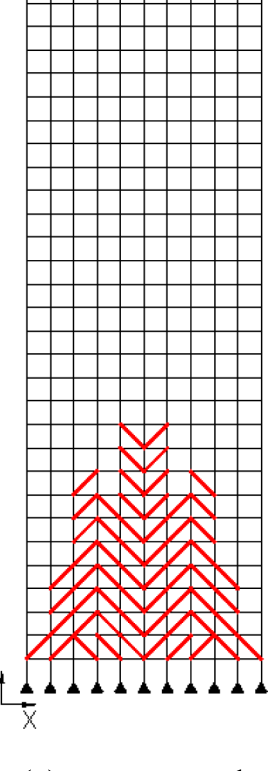


Fig. 2 Schematic of a 2D structure









(c) $m_n = 3000 \text{ kg}$

Fig. 3 Optimal damper layouts in the 2D frame structure with different floor masses in Example 1



206 Page 8 of 19 Z. Ou et al.

Table 1 Details of layout optimization with different floor masses in Example 1

Mass value of each node	Converged objective value	Iteration steps	CPU time (s)
600 kg	9.4674×10 ⁻⁶	163	12,245.04
2200 kg	4.8291×10^{-5}	157	15,758.24
3000 kg	7.0402×10^{-5}	161	18,679.42

is employed to optimize the layout of diagonally braced dampers in the 2D frame structure, aiming to minimize the maximum inter-story drift variance across all floors of the boundary columns. In order to ensure the aesthetics of the structure, bilateral symmetry constraints (Xie et al. 2020) will be added to the optimization process of this example,

and the symmetry axis is shown in Fig. 2. It is worth noting that the accuracy and efficiency of the NPDFRM algorithm have been demonstrated in Wu et al. (2022), and will not be repeated in this paper.

Under the specified maximum number of dampers, the optimal damper layouts of the 2D structure with different floor masses are shown in Fig. 3. It can be observed that, under the same seismic excitation, the layout optimization results for structures with different floor masses are very similar. The mass of the floor has little effect on the layout optimization results. The detailed computing performance is illustrated in Table 1. The change history of the objective function and the number of dampers is shown in Fig. 4. It can be seen that with the increase of floor mass, the influence of seismic excitation also increases, resulting in the increase of the objective function values. Meanwhile, additional time

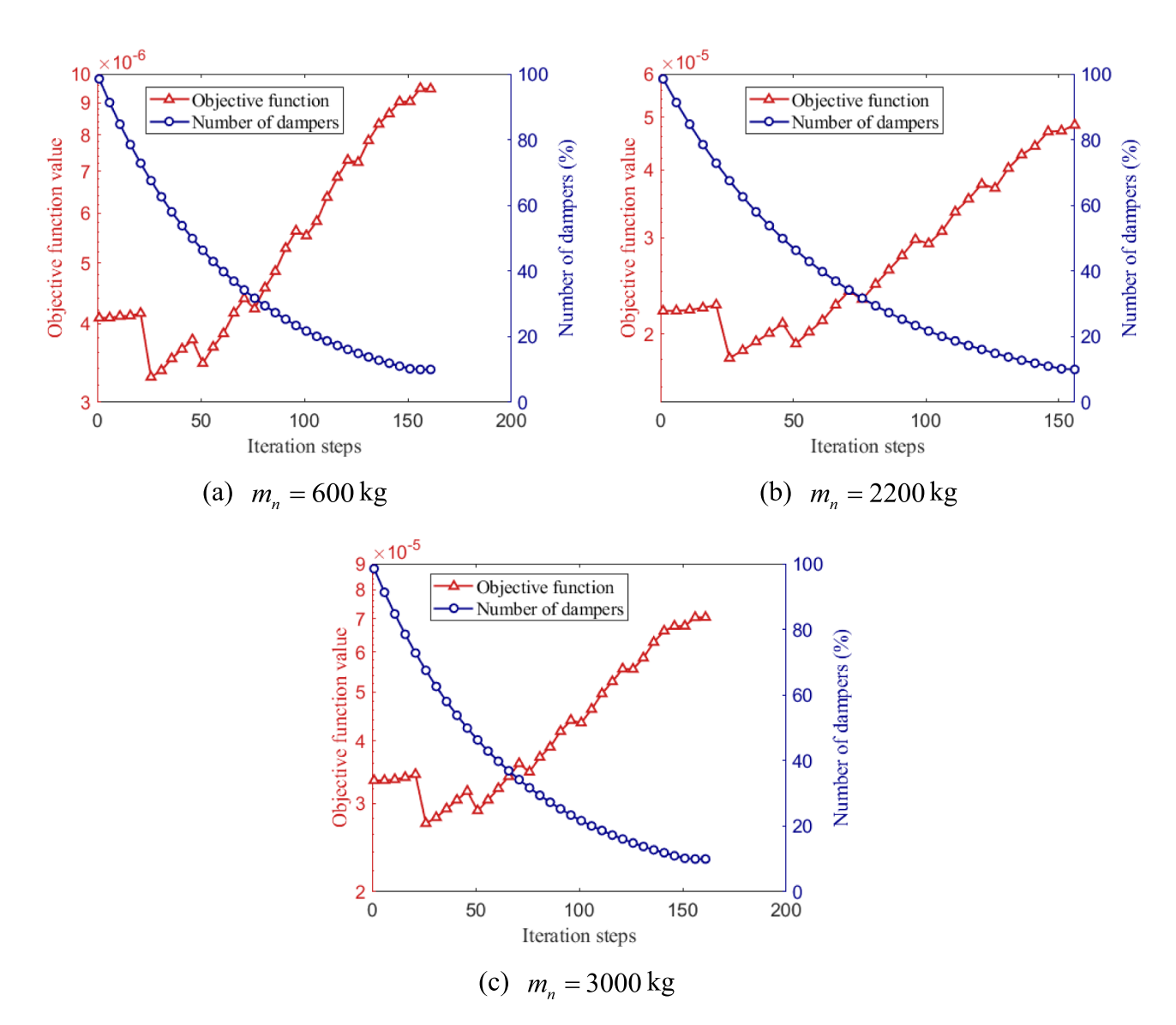


Fig. 4 Optimization history of the objective function and the number of dampers in Example 1



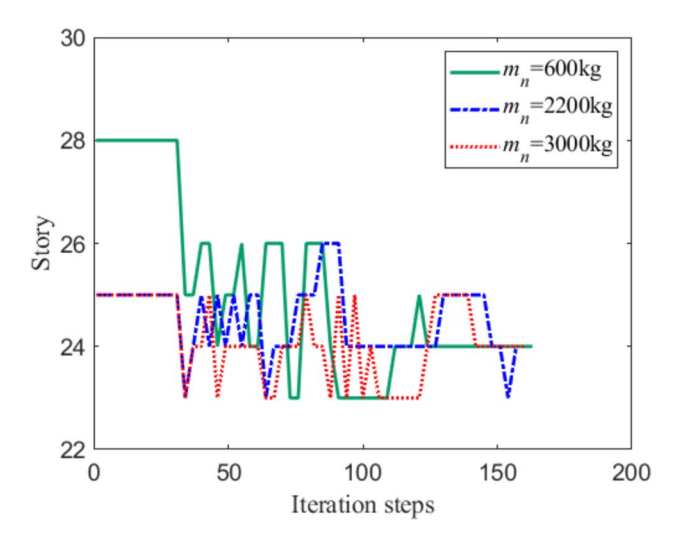
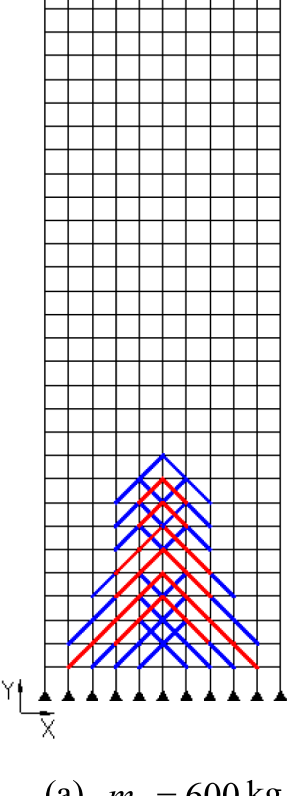


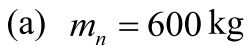
Fig. 5 Optimization history of the floor location of maximum drift variance in Example 1

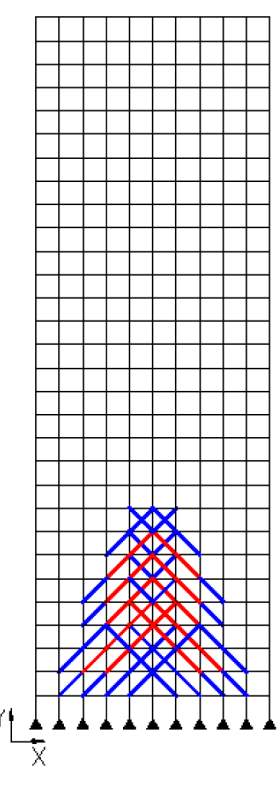
is required to compute more lower-order modes, increasing the CPU time required for layout optimization. The change history of the floor where the maximum inter-story drift variance is located is shown in Fig. 5. As shown in Figs. 4

and 5, there is a difference in the maximum inter-story drift variance and its specific floor location in structures with different floor masses. This difference is also reflected in the final results.

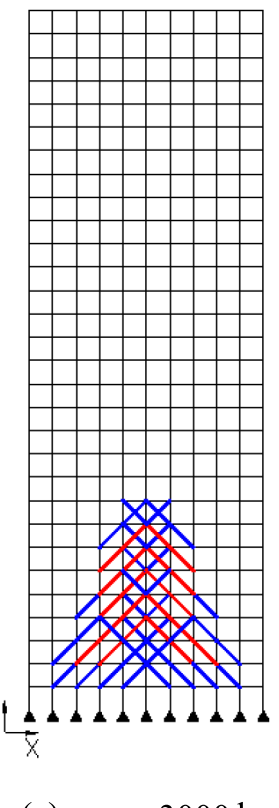
Next, we consider the layout optimization problem for two types of dampers as shown in Fig. 2, with damping coefficients of $c_1 = 1 \times 10^6 \,\mathrm{N} \cdot s/m$ (red line) and $c_2 = 1 \times 10^5 \,\mathrm{N} \cdot s/m$ (blue line). The quantities of c_1 and c_2 dampers used are limited to 4% and 6% of the total number of dampers, respectively. The optimal layout of two types of dampers for 2D structures with different floor masses, within the specified maximum number of each type of damper, is shown in Fig. 6. Compared with the optimized layout of one type of damper, the optimized layouts of the two types of dampers remain similar. The detailed computational performance is presented in Table 2. In Fig. 7, the evolution of the objective function and the number of dampers over time are illustrated. A comparison of Tables 1 and 2 reveals that the convergence objective function value in Table 2 is higher than that in Table 1. This increase occurs because more dampers with $c_2 = 1 \times 10^5 \,\mathrm{N} \cdot s/m$ are used, while fewer dampers with $c_1 = 1 \times 10^6 \,\mathrm{N} \cdot s/m$ are installed. Although this reduces the seismic resistance of the building structure, it also reduces its cost.







(b)
$$m_n = 2200 \,\mathrm{kg}$$



(c) $m_n = 3000 \text{ kg}$

Fig. 6 Optimal layouts of two damper types in the 2D frame structure with different floor masses in Example 1



206 Page 10 of 19 Z. Ou et al.

 $\begin{tabular}{ll} \textbf{Table 2} & Details of layout optimization with different floor masses in Example 1 \end{tabular}$

Mass value of each node	Converged objective value	Iteration steps	CPU time (s)
600 kg	1.5636×10^{-5}	186	13,199.54
2200 kg	7.3705×10^{-5}	187	17,711.70
3000 kg	1.0440×10^{-4}	188	22,073.66

Subsequently, we apply the diversified design technique (Xie 2025) to the aforementioned 2D structure with two damper types and $m_n = 600$ kg. The results of three random experiments on the optimal layout of dampers are shown in Fig. 8. By comparing the layouts of Figs. 6a

and 8, it can be seen that under the same initial layout, their optimal designs are similar. These results indicate the convex-like behavior of this layout optimization problem. Table 3 presents detailed computational performance. Figure 9 illustrates the variation history of the objective function and the number of dampers in the three random experiments. By comparing their convergence objective function values, it can be seen that two of the random experiment results have smaller convergence objective function values. Therefore, the diversified design technique can generate results that are closer to the global optimum solution.

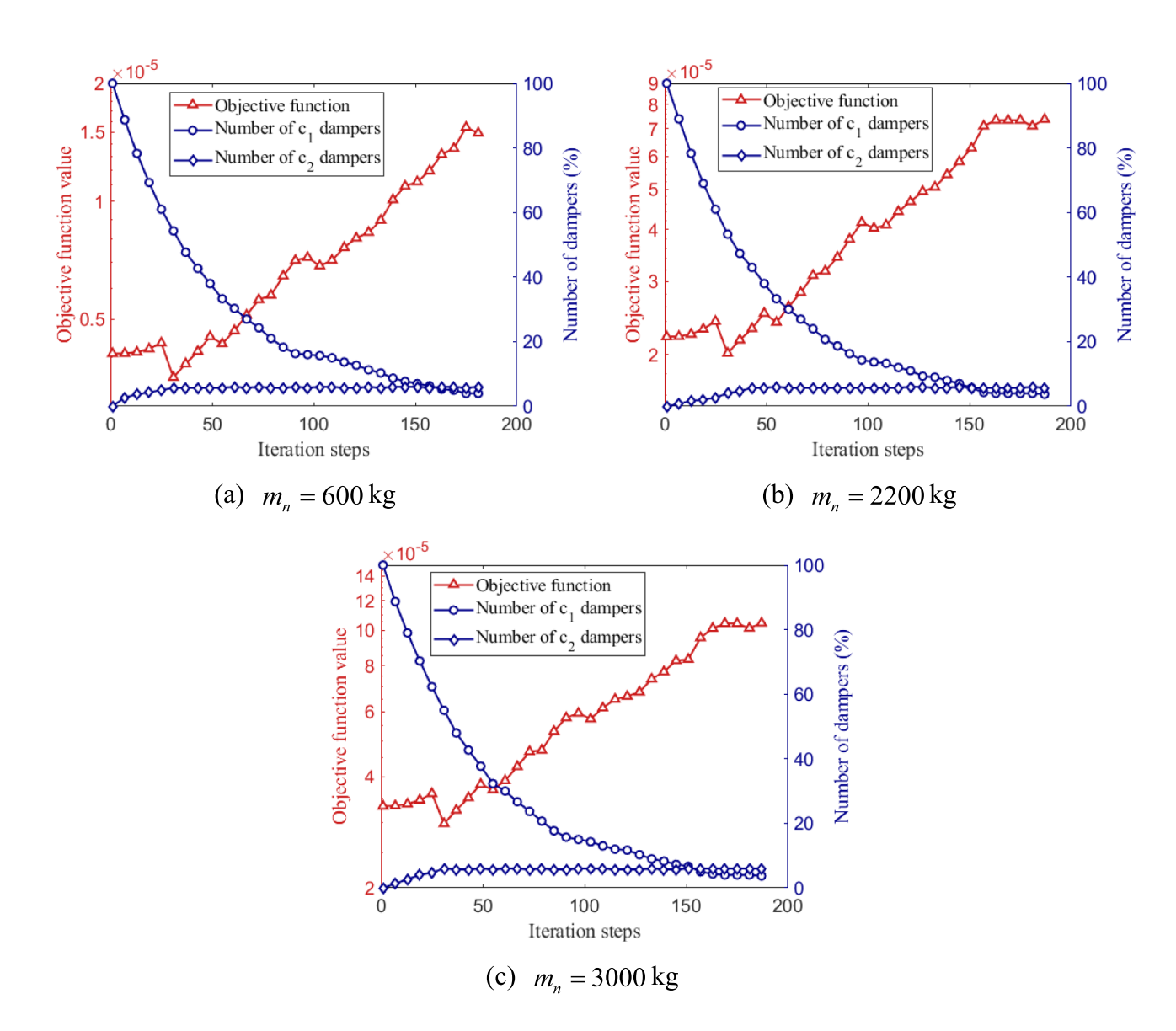


Fig. 7 Optimization history of the objective function and the number of two damper types in Example 1



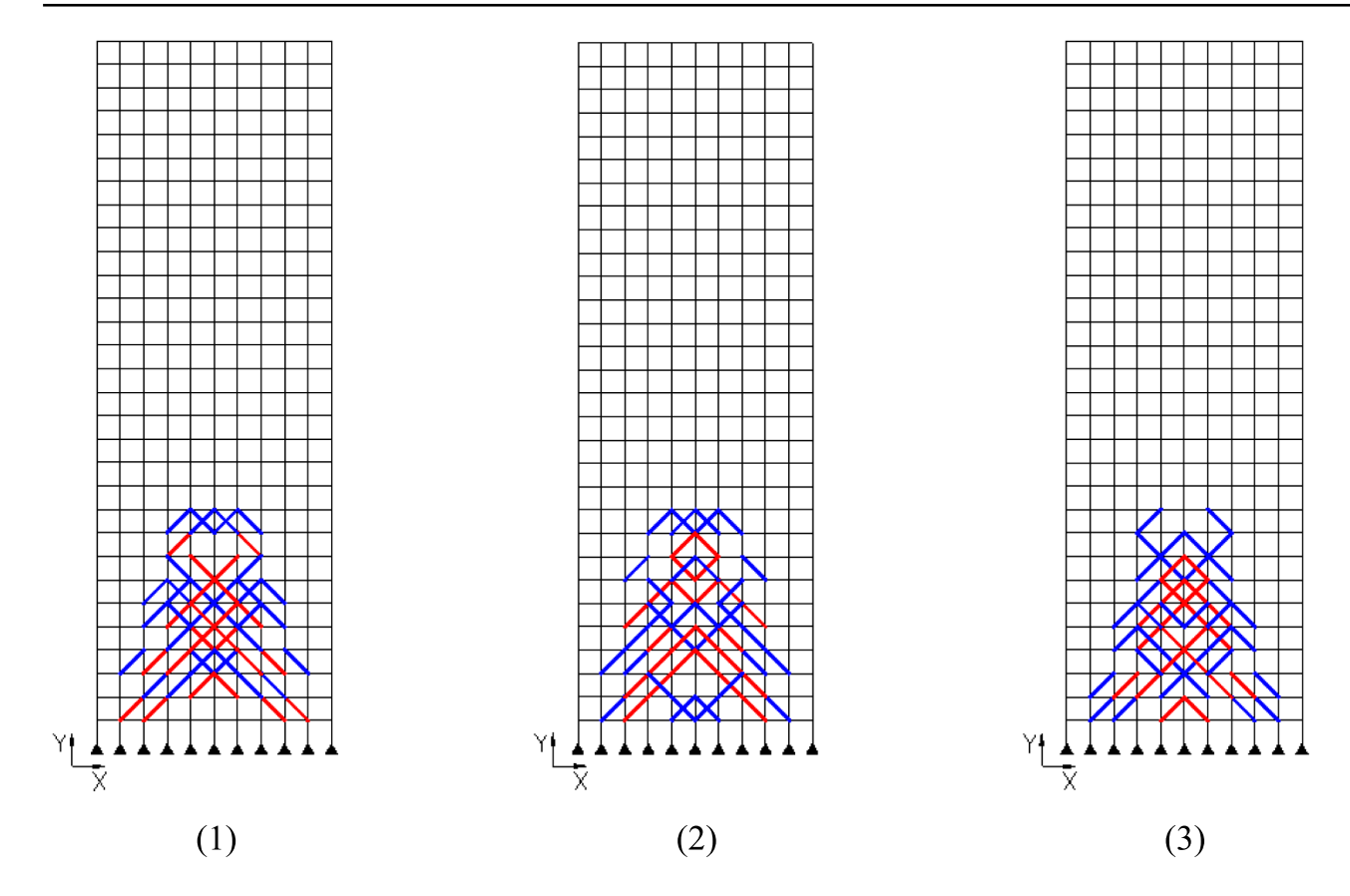


Fig. 8 Three random experiment results for optimal damper layouts in the 2D structure with two damper types and $m_n = 600$ kg in Example 1

4.2 Example 2: 3D frame structure

In the second example, a 3D steel frame structure with 4 bays on one side and 6 bays on the other, consisting of 20 story floors as depicted in Fig. 10, is investigated. Each black line in Fig. 10a–d represents a beam. Figure 10e shows the cross-section of the beam. Initially, dampers are installed on the front and rear surfaces of the structure (surfaces 1 and 5 in Fig. 10d) in two groups of 240 each. Here, dampers with a vertical span of one floor and a horizontal span of one bay are installed. In Fig. 10a-d, every red line represents a damper, and the damping coefficient is set as $c_1 = 1 \times 10^6 \,\mathrm{N} \cdot s/m$. The finite element model of the structure consists of 4410 DOFs. In this example, the seismic

Table 3 Details of three random experiments on the optimal layout of dampers for the 2D structure with two damper types and $m_n = 600 \text{ kg}$ in Example 1

Random experiment	Converged objective value	Iteration steps	CPU time (s)
(1)	1.5620×10^{-5}	185	12,635.74
(2)	1.5625×10^{-5}	182	12,558.45
(3)	1.6105×10^{-5}	174	12,000.64

excitation is eccentric, at an angle of 30 degrees to the X-axis and 60 degrees to the Y-axis. We consider the optimization problem of damper arrangement in the 3D structure containing three types of dampers, aiming to minimize the maximum inter-story drift variance among all floors of the middle column on the right side. The damping coefficients of the dampers used are $c_1 = 1 \times 10^6 N \cdot s/m$ (red line), $c_2 = 5 \times 10^5 \, \text{N} \cdot \text{s/m}$ (blue line) and $c_3 = 1 \times 10^5 \, \text{N} \cdot \text{s/m}$ (green line). The number of c_1 , c_2 and c_3 dampers used is limited to 4%, 3% and 3% of the total number of dampers, respectively. The layout optimization in this example will add the quarter-periodic symmetry constraints (Huang and Xie 2008) to preserve the aesthetics of the structure, with the symmetry axes shown in Fig. 10b, c.

The optimal layout of three types of dampers is shown in Fig. 11. Since the 3D structure in this example is symmetrical from front to back, only the main view of the layout optimization result is illustrated. Under the same seismic excitation, the optimal layouts of the three types of dampers are similar across structures with different floor masses. Table 4 lists the detailed calculation performance. As the floor mass increases, more low-order modes need to be calculated, thereby increasing the CPU time required for layout optimization. The variation history of the objective function



206 Page 12 of 19 Z. Ou et al.

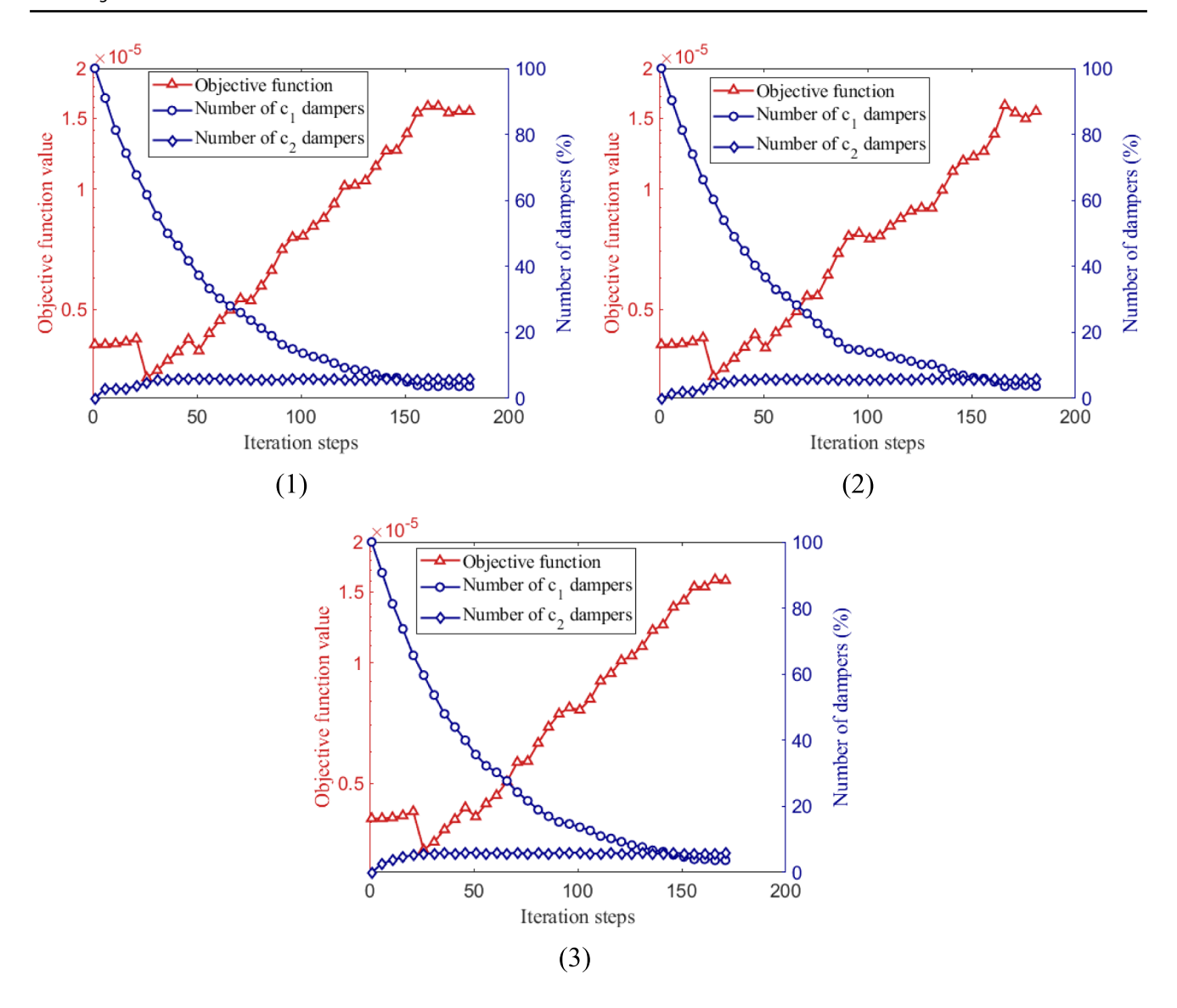


Fig. 9 Optimization history of the objective function and the number of dampers in the three random experiments for the 2D structure with two damper types and $m_n = 600 \text{ kg}$ in Example 1

value and the number of dampers is shown in Fig. 12. In addition, Fig. 13 shows the history of the floor where the maximum drift variance is located. In this example, it is evident that the optimization histories for the floors exhibiting the maximum inter-story drift variance are similar.

Similarly, we explore the diversified design technique for the 3D structure with three damper types and $m_n = 600$ kg. Figure 14 displays the results of three random experiments on the optimal layout of dampers. By comparing Fig. 11a with Fig. 14, it can be observed that their optimal layouts are similar under the same initial layout. These results also point out the convex-like behavior

of this layout optimization problem. Table 5 presents detailed computational performance. Figure 15 illustrates the variation history of the objective function and the number of dampers in the three random experiments. By comparing their converged objective function values, we can see that in this example, the converged objective function value of the original example is smaller and closer to the global optimum solution. It is worth noting that, because the diversified design technique involves randomness, running multiple calculations may yield an even lower objective function value.



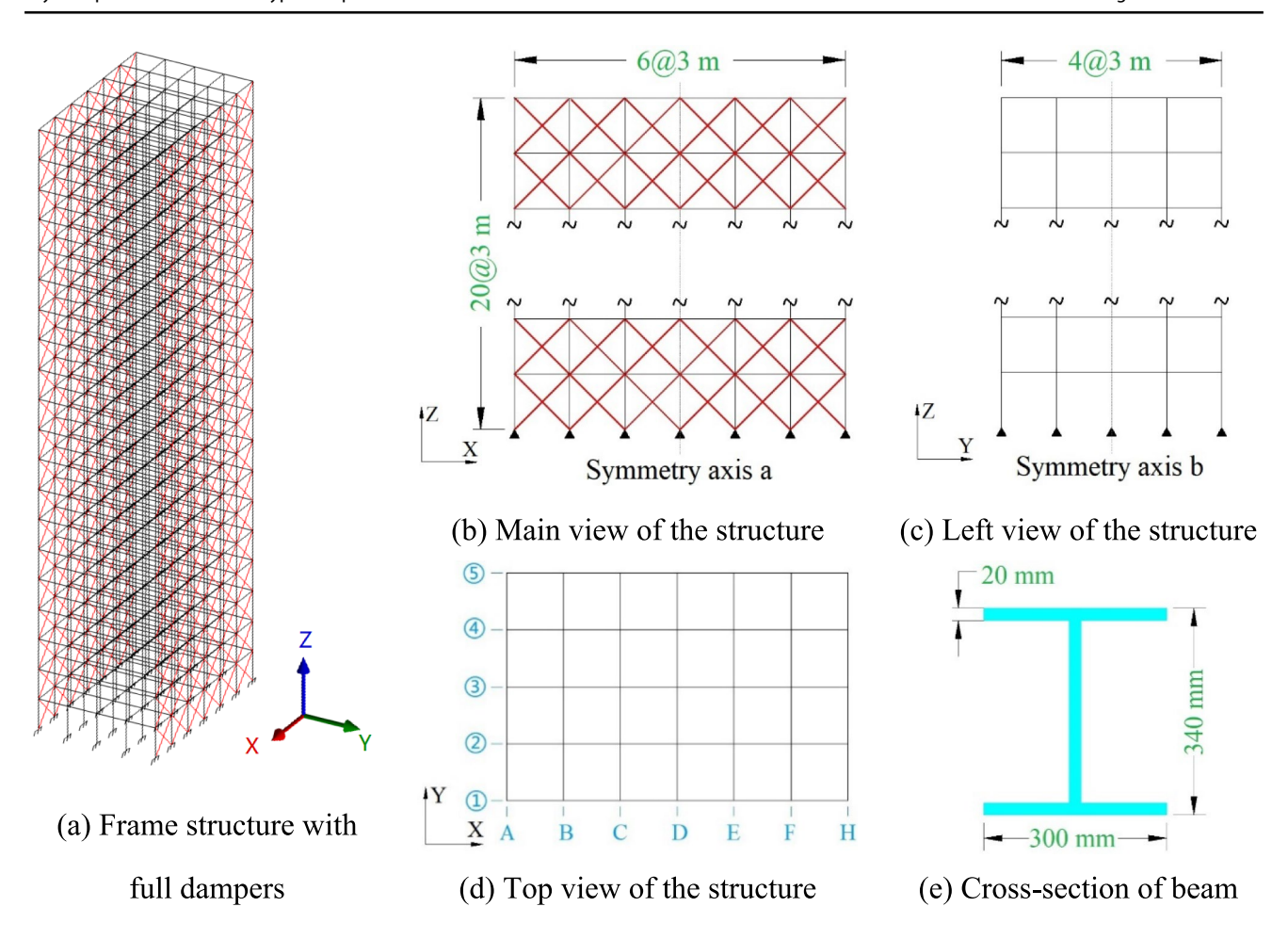


Fig. 10 Schematic of a 3D frame structure

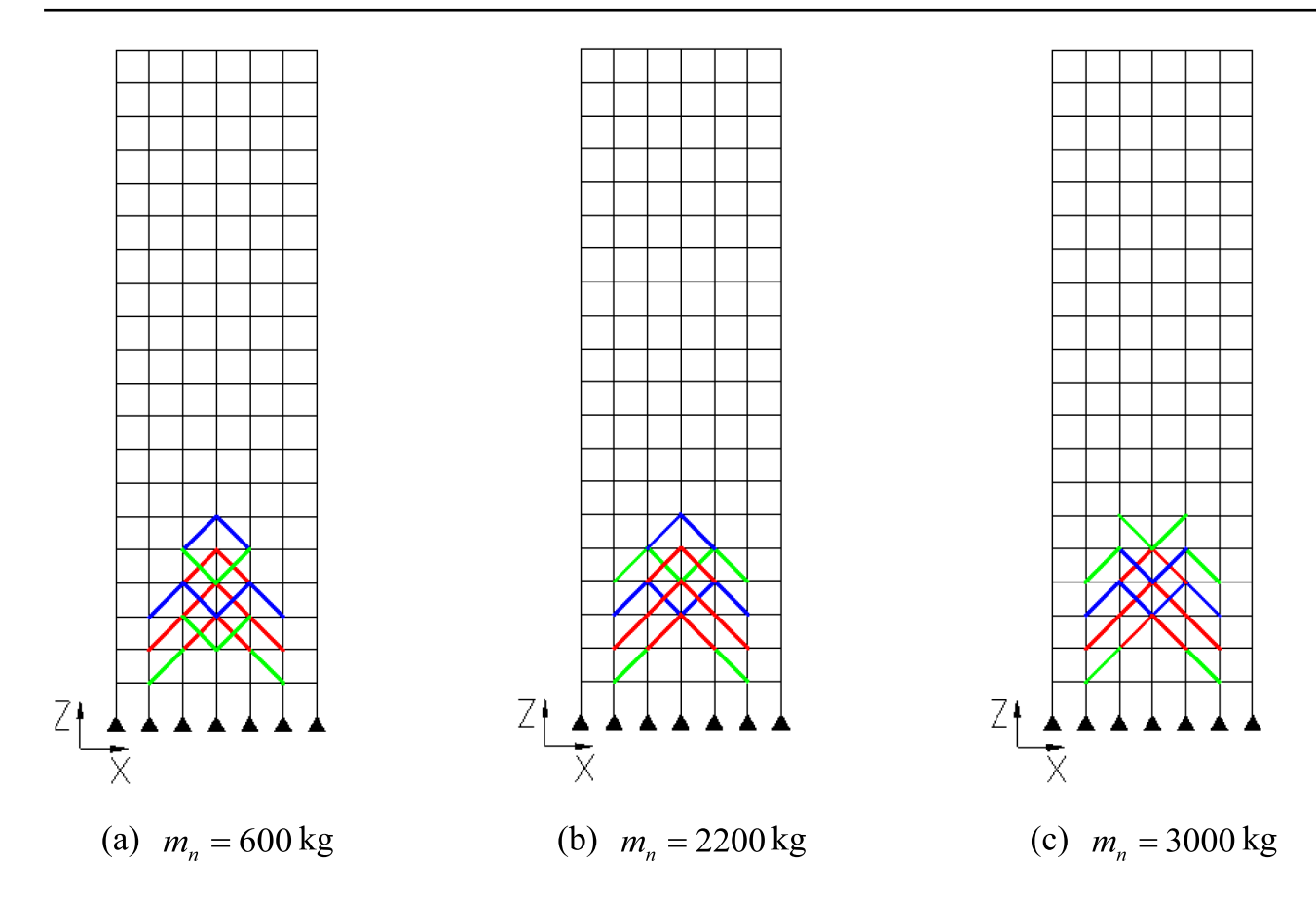
5 Conclusion

A new BESO-based optimization method is introduced to determine the layout of multi-type dampers in structures subjected to seismic excitation, with a constraint on the maximum number of each type of dampers. This approach integrates PEM with NPDFRM to adaptively calculate the inter-story drift variance across all floors of non-proportionally damped structures, ensuring both accuracy and efficiency in assessing the stochastic seismic response. In addition, the KS function is utilized to minimize the maximum inter-story drift variance among the boundary columns, facilitating the determination of the optimal layout of multi-type dampers. The proposed method is validated through two numerical examples involving

2D and 3D frame structures. The results demonstrate that this method effectively determines the optimal layout of multi-type dampers for structures with varying floor masses while adhering to the maximum limits for each type of damper. This approach can also serve as a practical tool for optimizing damper layouts in earthquake-prone regions. The present study has focused on the layout optimization problem of multi-type linear viscous dampers. As the number of damper types increases, this approach can effectively achieve simultaneous optimization of both damper parameters and layouts. Future research will investigate the generalization of the proposed method for non-stationary random responses.



206 Page 14 of 19 Z. Ou et al.



 $\textbf{Fig. 11} \quad \text{Optimal layouts of three damper types in the 3D structure with different floor masses in Example 2}$

 $\begin{tabular}{ll} \textbf{Table 4} & Details of layout optimization with different floor masses in Example 2 \end{tabular}$

Mass value of each node	Converged objective value	Iteration steps	CPU time (s)
600 kg	5.8932×10^{-6}	208	25,417.16
2200 kg	1.7481×10^{-5}	173	62,536.47
3000 kg	2.4962×10^{-5}	150	83,693.92



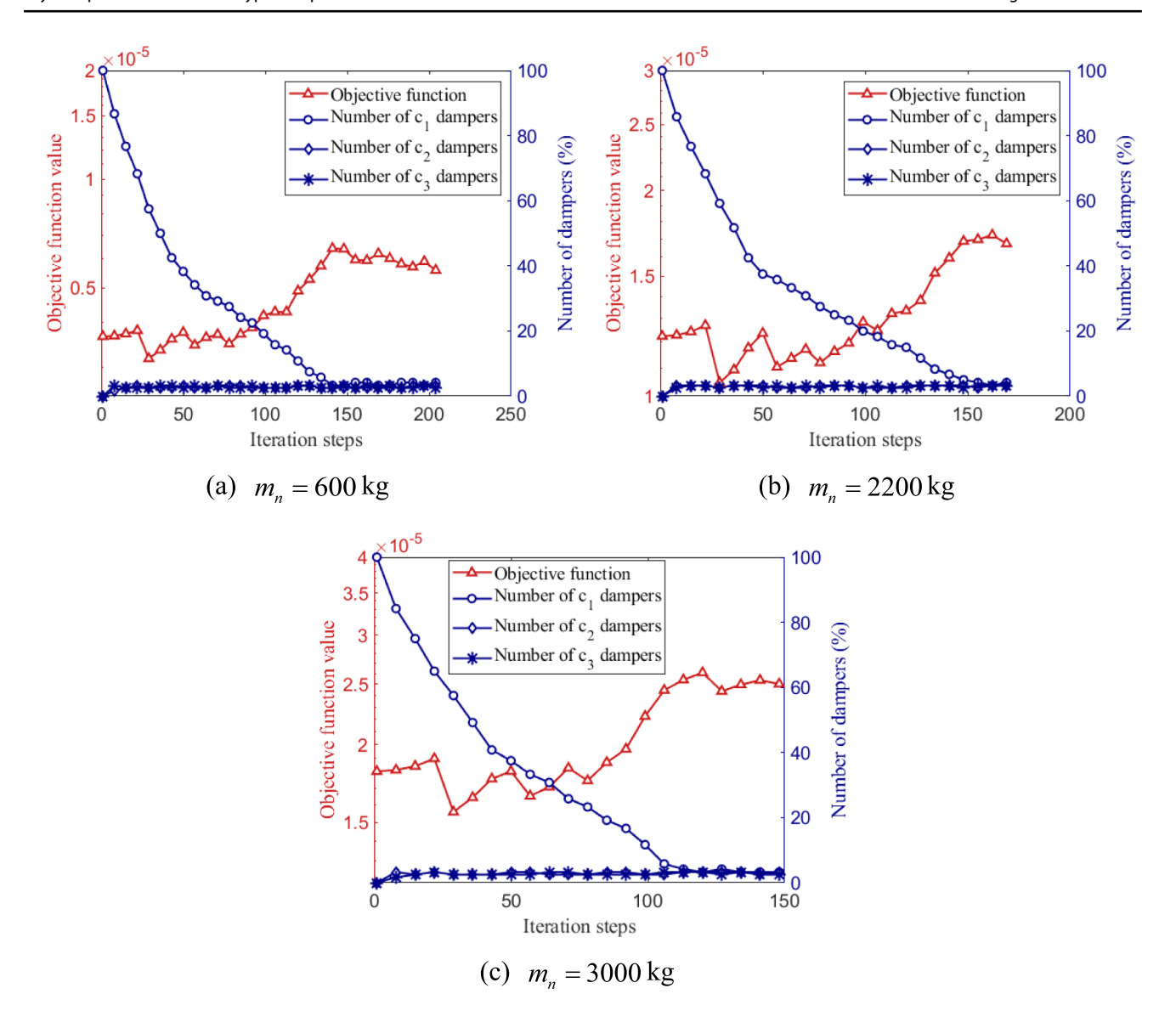


Fig. 12 Optimization history of the objective function and the number of dampers in Example 2



206 Page 16 of 19 Z. Ou et al.

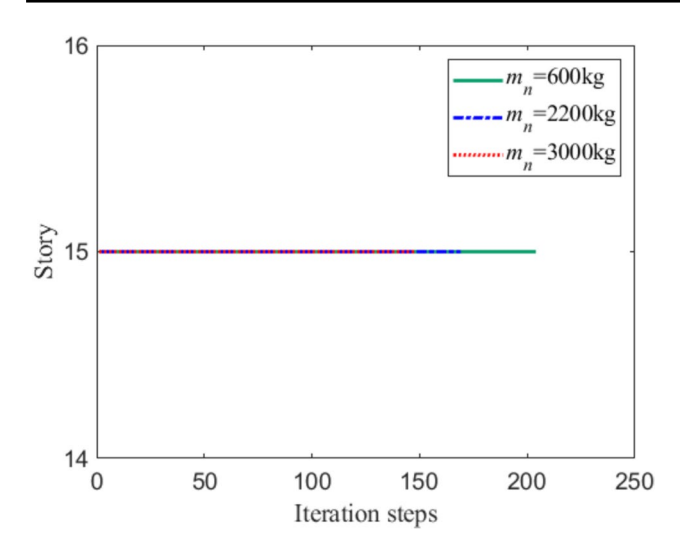


Fig. 13 Optimization history of the floor location of maximum drift variance in Example $\boldsymbol{2}$

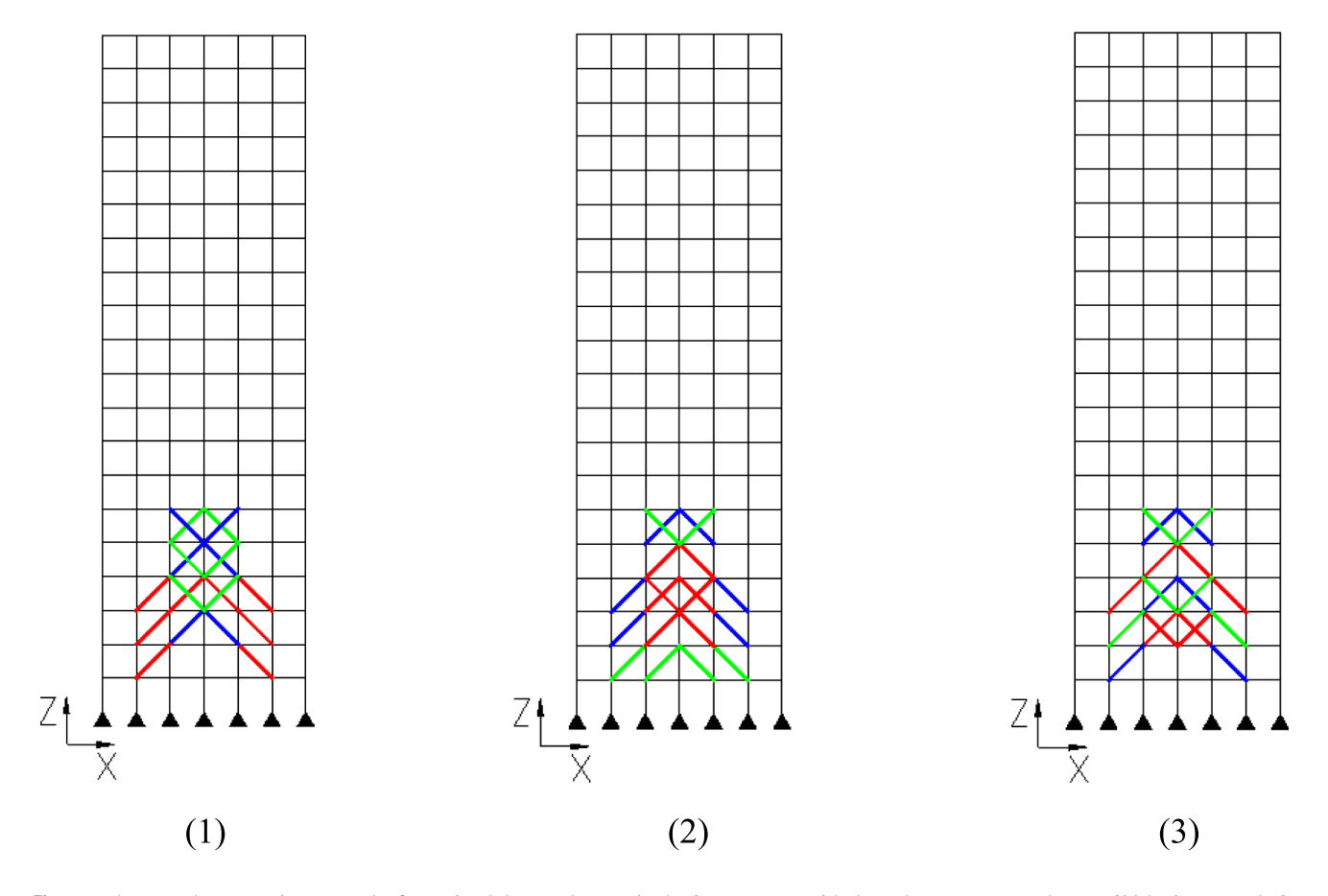


Fig. 14 Three random experiment results for optimal damper layouts in the 3D structure with three damper types and $m_n = 600 \text{ kg}$ in Example 2



Table 5 Details of three random experiments on the optimal layout of dampers in the 3D structure with three damper types and $m_n = 600$ kg in Example 2

Random experiment	Converged objective value	Iteration steps	CPU time (s)
(1)	6.2906×10 ⁻⁶	147	21,085.34
(2)	6.0506×10^{-6}	191	24,825.23
(3)	6.0983×10^{-6}	162	23,807.16

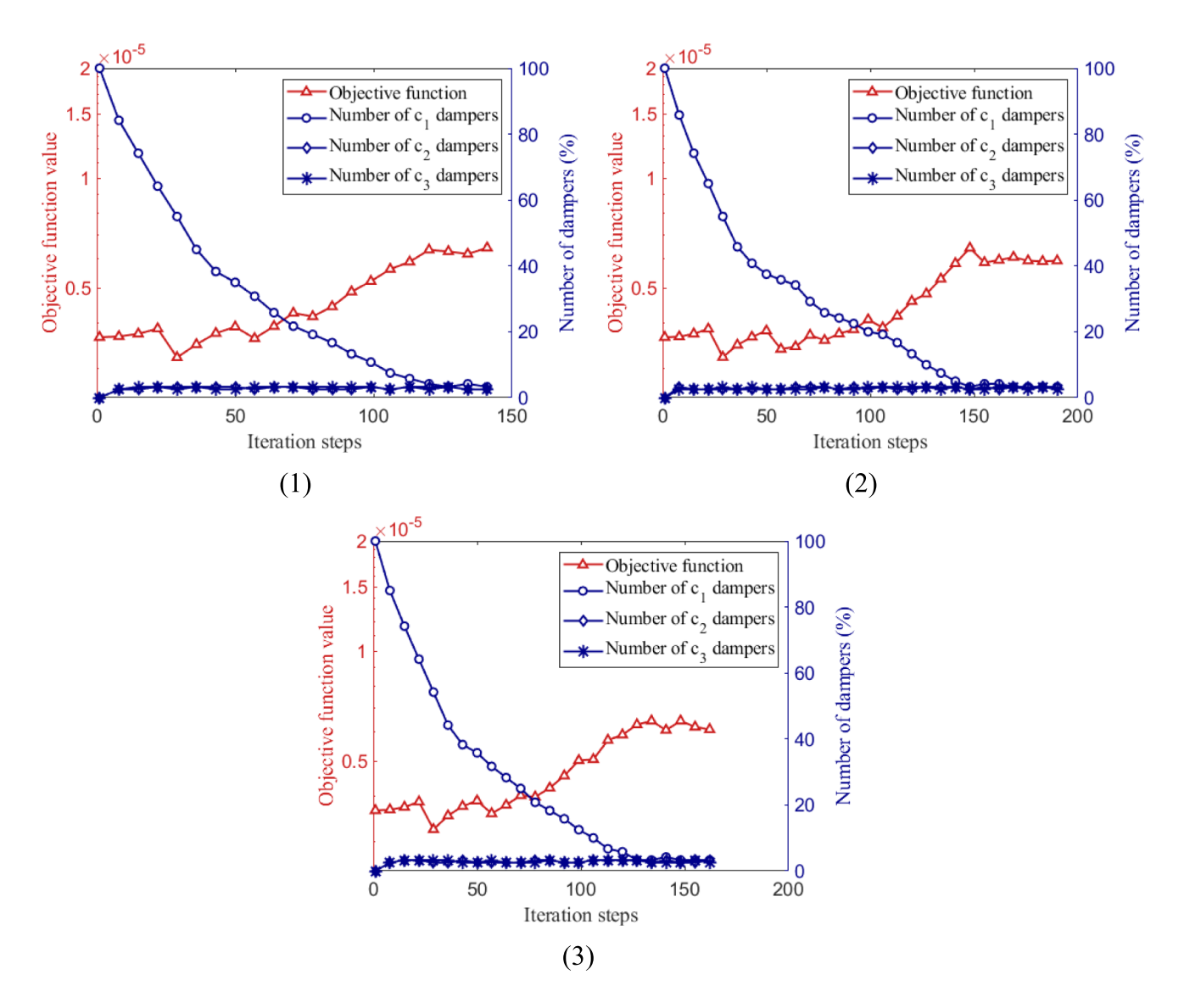


Fig. 15 Optimization history of the objective function and the number of dampers in the three random experiments for the 3D structure with three damper types and $m_n = 600 \text{ kg}$ in Example 2



Acknowledgments The work was supported by the Theme-based Research Scheme from the Research Grants Council of Hong Kong (Project No. T22-501/23-R). We would also like to thank the anonymous reviewers for their comments.

Author contributions Zhihao Ou: Methodology, Investigation, Software, Writing-Original Draft; Baisheng Wu: Conceptualization, Methodology, Investigation, Writing-Review & Editing; Siu-Kai Lai: Methodology, Investigation, Funding Acquisition, Writing-Review & Editing; Zeyao Chen: Methodology, Investigation, Validation, Writing-Review & Editing.

Funding Open access funding provided by The Hong Kong Polytechnic University. The work was supported by the Theme-based Research Scheme from the Research Grants Council of Hong Kong (Project No. T22-501/23-R).

Data availability Data will be made available upon reasonable request from the authors.

Declarations

Conflict of interest The authors declare that they have no known competing financial interests or personal relationships that could have appeared to influence the work reported in this paper.

Replication of results The numerical results presented in this study can be reproduced using the topology optimization algorithm proposed herein. Additional information is available upon reasonable request.

Open Access This article is licensed under a Creative Commons Attribution 4.0 International License, which permits use, sharing, adaptation, distribution and reproduction in any medium or format, as long as you give appropriate credit to the original author(s) and the source, provide a link to the Creative Commons licence, and indicate if changes were made. The images or other third party material in this article are included in the article's Creative Commons licence, unless indicated otherwise in a credit line to the material. If material is not included in the article's Creative Commons licence and your intended use is not permitted by statutory regulation or exceeds the permitted use, you will need to obtain permission directly from the copyright holder. To view a copy of this licence, visit http://creativecommons.org/licenses/by/4.0/.

References

- Alavi B, Krawinkler H (2004) Strengthening of moment-resisting frame structures against near-fault ground motion effects. Earthq Eng Struct Dyn 33(6):707–722. https://doi.org/10.1002/eqe.370
- Bendsøe MP, Kikuchi N (1998) Generating optimal topologies in structural design using a homogenization method. Comput Methods Appl Mech Eng 71(2):197–224. https://doi.org/10.1016/0045-7825(88)90086-2
- Bourdin B (2001) Filters in topology optimization. Int J Numer Methods Eng 50(9):2143–2158. https://doi.org/10.1002/nme.116
- Chen A, Lin X, Zhao ZL, Xie YM (2023) Layout optimization of steel reinforcement in concrete structure using a truss-continuum model. Front Struct Civ Eng 17(5):669–685. https://doi.org/10.1007/s11709-023-0963-0
- Chopra AK (1995) Dynamics of structures: theory and applications to Earthquake engineering. Hall International Inc, Des Moines
- Clough RW, Penzien J (1975) Dynamics of structures. Mc Graw-Hill Inc, New York
- $\underline{\underline{\mathscr{D}}}$ Springer

- D'Amico B, Pomponi F (2020) On mass quantities of gravity frames in building structures. J Build Eng 31:101426. https://doi.org/10.1016/j.jobe.2020.101426
- European Committee for Standardization (2004) Eurocode 8: design of structures for earthquake resistance
- Gao W, Lu X, Wang S (2022) Seismic topology optimization based on spectral approaches. J Build Eng 47:103781. https://doi.org/10.1016/j.jobe.2021.103781
- Gomez F, Spencer BF Jr, Carrion J (2021) Simultaneous optimization of topology and supplemental damping distribution for buildings subjected to stochastic excitation. Struct Control Health Monit 28(7):e2737. https://doi.org/10.1002/stc.2737
- Haftka RT, Gürdal Z (1992) Elements of structural optimization, 3rd edn. Springer, Dordrecht
- Housner GW, Bergman LA, Caughey TK, Chassiakos AG, Claus RO, Masri SF, Skelton RE, Soong TT, Spencer BF, Yao JT (1997) Structural control: past, present, and future. ASCE J Eng Mech 123(9):897–971. https://doi.org/10.1061/(ASCE) 0733-9399(1997)123:9(897)
- Huang X, Xie YM (2008) Optimal design of periodic structures using evolutionary topology optimization. Struct Multidisc Optim 36:597–606. https://doi.org/10.1007/s00158-007-0196-1
- Huang X, Xie YM (2009) Bi-directional evolutionary topology optimization of continuum structures with one or multiple materials. Comput Mech 43(3):393–401. https://doi.org/10.1007/s00466-008-0312-0
- Huang C, Liu ZS, Chen SH (1997) An accurate modal method for computing response to periodic excitation. Comput Struct 63(3):625-631. https://doi.org/10.1016/S0045-7949(96) 00367-7
- International Conference of Building Officials (ICBO) (1997) 1997 Uniform Building Code, vol 2. Whittier, CA, USA
- Kreisselmeier G, Steinhauser R (1979) Systematic control design by optimizing a vector performance index. IFAC Proc Vol 12(7):113–117. https://doi.org/10.1016/S1474-6670(17)65584-8
- Lavan O, Amir O (2014) Simultaneous topology and sizing optimization of viscous dampers in seismic retrofitting of 3D irregular frame structures. Earthq Eng Struct Dyn 43(9):1325–1342. https://doi.org/10.1002/eqe.2399
- Li L, Hu YJ, Wang XL, Lü L (2014) A hybrid expansion method for frequency response functions of non-proportionally damped systems. Mech Syst Signal Process 42(1/2):31–41. https://doi.org/10. 1016/j.ymssp.2013.07.020
- Li L, Hu YJ, Wang XL (2016) Accurate method for harmonic responses of non-classically damped systems in the middle frequency range. J Vib Control 22(2):426–441. https://doi.org/10. 1177/1077546314533579
- Li C, Wang R, Jiang L, Huang B, Ge X (2023) Dynamic analysis of damping structures considering support stiffness. Structures 57:105297. https://doi.org/10.1016/j.istruc.2023.105297
- Lin JH, Zhao Y, Zhang YH (2001) Accurate and highly efficient algorithms for structural stationary/non-stationary random responses. Comput Methods Appl Mech Eng 191:103–111. https://doi.org/10.1016/S0045-7825(01)00247-X
- Liu Q, Paavola J (2015) Drift reliability-based optimization method of frames subjected to stochastic earthquake ground motion. Appl Math Model 39(3–4):982–999. https://doi.org/10.1016/j. apm.2014.07.021
- Liu ZS, Wang K, Huang C, Chen SH (1996) An extended hybrid method for contribution due to truncated lower- and higher-frequency modes in modal summation. Eng Struct 18(7):558–563. https://doi.org/10.1016/0141-0296(95)00123-9
- Liu H, Zhang W, Gao T (2015) A comparative study of dynamic analysis methods for structural topology optimization under harmonic force excitations. Struct Multidisc Optim 51(6):1321– 1333. https://doi.org/10.1007/s00158-014-1218-4

- Luo Y, Bao J (2019) A material-field series-expansion method for topology optimization of continuum structures. Comput Struct 225:106122. https://doi.org/10.1016/j.compstruc.2019.106122
- Moghaddam H, Hajirasouliha I, Doostan A (2005) Optimum seismic design of concentrically braced steel frames: concepts and design procedures. J Constr Steel Res 61(2):151-166. https:// doi.org/10.1016/j.jcsr.2004.08.002
- National Standard of the People's Republic of China (2010) Code for seismic design of buildings (GB50011-2010). Architecture and Building Press, Beijing
- Ou Z, Wu B, Lai SK, Zhao X, Zhong H (2025) Topology optimization of structures under band harmonic excitation using improved adaptive quadrature method. Eng Struct 326:119528. https://doi.org/10.1016/j.engstruct.2024.119528
- Pollini N, Lavan O, Amir O (2017) Minimum-cost optimization of nonlinear fluid viscous dampers and their supporting members for seismic retrofitting. Earthq Eng Struct Dyn 46(2):1941-1961. https://doi.org/10.1002/eqe.2888
- Pozo S, Gomez F, Golecki T, Carrion J, Spencer BF Jr (2023) TopSTO: a 115-line code for topology optimization of structures under stationary stochastic dynamic loading. Earthq Eng Eng Vib 22(4):1081-1100. https://doi.org/10.1007/ s11803-023-2219-3
- Ou ZO (2000) Hybrid expansion method for frequency responses and their sensitivities, part I: undamped systems. J Sound Vib 231(1):175-193. https://doi.org/10.1006/jsvi.1999.2672
- Qu ZQ, Selvam RP (2000) Hybrid expansion method for frequency responses and their sensitivities, part II: viscously damped systems. J Sound Vib 238(3):369-388. https://doi.org/10.1006/jsvi.
- Sigmund O, Petersson J (1998) Numerical instabilities in topology optimization: a survey on procedures dealing with checkerboards, mesh-dependencies and local minima. Struct Multidisc Optim 16(1):68-75, https://doi.org/10.1007/BF01214002
- Soong TT, Spencer BF (2002) Supplemental energy dissipation: stateof-the-art and state-of-the-practice. Eng Struct 24(3):243-259. https://doi.org/10.1016/S0141-0296(01)00092-X
- Su C, Xian J (2022) Topology optimization of non-linear viscous dampers for energy-dissipating structures subjected to nonstationary random seismic excitation. Struct Multidisc Optim 65(7):200. https://doi.org/10.1007/s00158-022-03281-2

- Su C, Huang H, Ma H (2016) Fast equivalent linearization method for nonlinear structures under nonstationary random excitations. J Eng Mech 142(8):04016049. https://doi.org/10.1061/(ASCE)EM. 1943-7889.000109
- Symans MD, Charney FA, Whittaker AS, Constantinou MC, Kircher CA, Johnson MW, McNamara RJ (2008) Energy dissipation systems for seismic applications: current practice and recent developments. ASCE J Struct Eng 134(1):3-21. https://doi.org/10.1061/ (ASCE)0733-9445(2008)134:1(3)
- Traill-Nash RW (1981) Modal methods in the dynamics of systems with non-classical damping. Earthq Eng Struct Dyn 9(2):153–169. https://doi.org/10.1002/eqe.4290090205
- Wirsching PH, Paez TL, Ortiz K (2006) Random vibrations: theory and practice. Courier Corporation, New York
- Wu B, Zhao X, Lim CW, Zhong H (2022) Efficient computation of frequency response for non-proportional damped systems. Eng Struct 266:114636. https://doi.org/10.1016/j.engstruct.2022.114636
- Xie YM (2025) Generalized topology optimization for structural design. Springer Nature, New York
- Xie X, Wang S, Ye M, Xia Z, Zhao W, Jiang N, Xu M (2020) Isogeometric topology optimization based on energy penalization for symmetric structure. Front Mech Eng-Prc 15:100-122. https:// doi.org/10.1007/s11465-019-0568-4
- Yan K, Cheng G (2018) An adjoint method of sensitivity analysis for residual vibrations of structures subject to impacts. J Sound Vib 418:15-35. https://doi.org/10.1016/j.jsv.2017.12.015
- Zhao X, Wu B, Lai SK, Li Z, Zhong H (2021) A PEM-based topology optimization for structures subjected to stationary random excitations. Eng Struct 229(15):111613. https://doi.org/10.1016/j.engst ruct.2020.111613
- Zhao X, Wu B, Lai SK, Liu W, Zhong H (2022) Topology optimization of proportionally damped structures under harmonic excitations: analysis of velocity and acceleration responses. Eng Struct 258:114140. https://doi.org/10.1016/j.engstruct.2022.114140

Publisher's Note Springer Nature remains neutral with regard to jurisdictional claims in published maps and institutional affiliations.

